

## A direct approach to generalised Multiple Mapping Conditioning for selected turbulent diffusion flame cases

B. Sundaram<sup>a</sup>, A.Y. Klimenko<sup>a</sup>, M.J. Cleary<sup>b</sup>, Y. Ge<sup>c</sup>

<sup>a</sup> *The University of Queensland, School of Mechanical and Mining Engineering, QLD 4072, Australia*

<sup>b</sup> *The University of Sydney, School of Aerospace, Mechanical and Mechatronic Engineering, NSW 2006, Australia*

<sup>c</sup> *Institut für Thermodynamik, Fakultät für- und Raumfahrttechnik, Universität der Bundeswehr München, 85577 Neubiberg, Germany*

---

### Abstract

This work presents a direct and transparent interpretation of two concepts for modelling turbulent combustion: generalised Multiple Mapping Conditioning (MMC) and sparse-Lagrangian Large Eddy Simulation (LES). The MMC approach is presented as a hybrid between the probability density function (PDF) method and approaches based on conditioning (e.g. Conditional Moment Closure, flamelet, etc.). The sparse-Lagrangian approach, which allows for a dramatic reduction of computational cost, is viewed as an alternative interpretation of the Filtered Density Function (FDF) methods. This work presents simulations of several turbulent diffusion flame cases and discusses the universality of the localness parameter between these cases and the universality of sparse-Lagrangian FDF methods with MMC.

*Keywords:* Multiple Mapping Conditioning, Probability Density Function, Large Eddy Simulation, turbulent diffusion flames Flame.

---

*Email address:* [bruntha.sundaram@uqconnect.edu.au](mailto:bruntha.sundaram@uqconnect.edu.au) (B. Sundaram<sup>a</sup>)

## 1. Introduction

The complexities of modelling turbulent combustion, which involves non-linear, multi-scale interactions between turbulent fluctuations and chemistry, have been discussed in many publications [1, 2], and a number of approaches to the problem have been suggested. These approaches can be divided into two major categories: 1) those based on utilising the mixture fraction [3–5] in one way or the other; and 2) those involving modelling of joint PDFs of reactive scalars [6, 7]. The first category (fast chemistry, flamelet, Conditional Moment Closure (CMC), etc.) is characterised by relatively low computational cost, while the second category involves more general, albeit more computationally expensive methods. These two groups can be used in the context of both Reynolds Averaged Navier-Stokes (RANS) and Large Eddy Simulations (LES) [8–15]. A third option — Direct Numerical Simulation (DNS) — is a very useful tool but can hardly be used in complex practical applications due to prohibitive computational costs. The universality of probability density function (PDF) methods is based on the application of instantaneous non-linear chemical reaction rates, which thus appear in the model in closed form. However, the PDF equations contain unclosed conditional scalar dissipation terms, which necessitate the involvement of mixing models; Interaction by Exchange with the Mean (IEM) [16, 17], Curl’s [18], Modified Curl’s (MC) [19, 20] and Euclidean Minimum Spanning Tree (EMST) [21] are noted to be the most popular choices of mixing models.

The development of PDF methods in the last decade has resulted in the formulation of hybrid PDF models that allow us to combine the advantages and offset the disadvantages of the aforementioned categories. This development is based on conditioning of the mixing operator, which due to historic reasons, is called Multiple Mapping Conditioning (MMC). MMC allows us to use PDF

methods flexibly with the possibility of reducing computational cost and/or increasing quality of simulations by assigning useful properties introduced by other models onto the PDF model. A wide deployment of MMC methods was, to some extent, restricted by the complexity of the original MMC [22]. MMC has since evolved into a more flexible, generalised form [23, 24] and has been applied in many different ways [25–33]. We note here that original MMC is a special case of generalised MMC. In addition to properties considered later in this work, original MMC has some specific features that are discussed in the Appendix. It appears that more general forms of MMC allow for relatively simple and transparent interpretations of the model. This work does not present the chronological development of MMC and its various forms, but rather, a simpler, direct (and more efficient) generalised version of the MMC approach with illustrative flame cases.

The computationally economical versions of MMC are linked to the development of sparse methods [12, 34–36], whose introduction is related to MMC principles but generally represents an independent idea. For the MMC approach, we present a transparent, physical explanation of the sparse methods. We also explain the application of sparse-Lagrangian MMC for three cases, including a flamesheet [37], the Sandia D-F flame series [38] and the Cabra lifted hydrogen flame in a vitiated coflow [39].

## **2. A simple approach to generalised MMC**

This section takes an alternative, simpler approach to the introduction of MMC in its generalised form. For the sake of consistency and completeness, the original version of the MMC model is discussed in the Appendix. To maintain a simple presentation of the equations, a case of constant density and constant molecular diffusivity is considered, although MMC can of course be derived and

used for variable density and/or non-constant diffusivities (with the possibility of modelling the differential diffusion effects [40]).

### 2.1. Joint PDF equation

The primary requirement for every PDF model is consistency with the joint PDF equation (for example, see [4]) which can be conventionally written in the form,

$$\frac{\partial P_Y}{\partial t} + \nabla \cdot (\mathbf{u}_Y P_Y) + \frac{\partial W_I P_Y}{\partial y_I} + \frac{\partial^2 N_{IJ} P_Y}{\partial y_I \partial y_J} = D \nabla^2 P_Y. \quad (1)$$

Here  $P_Y(\mathbf{y}; \mathbf{x}, t)$  is the joint PDF of reactive scalars  $Y_1, \dots, Y_{n_s}$  that satisfy the conventional scalar transport equation,

$$\frac{\partial Y_I}{\partial t} + \nabla \cdot (\mathbf{v} Y_I) - D \nabla^2 Y_I = W_I, \quad (2)$$

where the indices  $I, J = 1, \dots, n_s$  run over the reactive scalars,  $\mathbf{u} = \mathbf{u}(\mathbf{x}, t)$  is the fluid velocity,  $\mathbf{u}_Y(\mathbf{y}; \mathbf{x}, t) = \langle \mathbf{u} | \mathbf{Y} = \mathbf{y}, \mathbf{x}, t \rangle$  is its conditional expectation,  $D$  is the diffusivity, which as noted above is assumed to be the same for all species,  $W_I = W_I(\mathbf{Y})$  is the reaction rate for species  $I$  and

$$N_{IJ}(\mathbf{y}; \mathbf{x}, t) \equiv \langle D \frac{\partial Y_I}{\partial x_k} \frac{\partial Y_J}{\partial x_l} | \mathbf{Y} = \mathbf{y}, \mathbf{x}, t \rangle \quad (3)$$

is the conditional scalar dissipation. In flows with high Reynolds numbers, the last term in Equation (1) is small and can be neglected. In general, our consideration is also applicable to joint scalar-velocity PDF transport equations [6], but in this work, we focus on investigating consistency of MMC models with "scalars-only" PDF transport equations. An important attribute of the PDF equation is that the chemical source terms appear in exact form and do not require additional closures.

## 2.2. Stochastic PDF models

Due to the large dimensionality of PDFs in reacting flows which usually involve tens of chemical species in hundreds of chemical reactions, a direct solution of PDF equations becomes extremely difficult and can practically be achieved only by stochastic simulations. Consider a stochastic system specified by the following differential equations of the Ito type:

$$d\mathbf{x}^* = \mathbf{U}(\boldsymbol{\xi}^*; \mathbf{x}^*, t)dt + (2D)^{1/2} d\boldsymbol{\omega}_x^*; \quad (4)$$

$$d\xi_k^* = A_k(\boldsymbol{\xi}^*; \mathbf{x}^*, t)dt + b_{kl}(\boldsymbol{\xi}^*; \mathbf{x}^*, t)d\omega_l^*; \quad (5)$$

$$dY_I^* = (W_I(\mathbf{Y}^*) + S_I^*)dt. \quad (6)$$

Most conventional PDF models [7] can be represented in the form of Equations (4)-(6). The velocities  $\mathbf{U}^*$  and positions  $\mathbf{x}^*$  in physical space evolve according to the model represented by a Markov family, where the symbol  $\omega$  is used to denote Wiener processes. The evolution of the simulated reactive scalars  $Y_I^*$  depends on reaction rates  $W_I$  and on a mixing operator, whose effect on  $Y_I^*$  is represented by  $S_I^*$ . The IEM, Curl's (original and modified) and EMST mixing models are common examples of conventional mixing operators. The values  $\xi_k^*$  can represent various physical quantities, such as velocities, accelerations, dissipations, mixture fraction(s) or additional variables used to emulate these quantities. In the context of MMC models, the variables  $\xi_k^*$  are referred to as *reference variables*. It is important to note that in MMC, the reference variables  $\xi_k^*$  must not coincide with the variables  $Y_I^*$  which simulate reacting scalars. Hence, a typical MMC model has two distinct mixture fractions: simulated and reference. As we wish to keep our consideration general, all these values are denoted as  $n_r$  stochastic variables  $\xi_1^*, \dots, \xi_{n_r}^*$ .

The stochastic system of Equations (4)-(6) corresponds to the Fokker-Planck

(direct Kolmogorov) equation,

$$\frac{\partial P_{Y\xi}}{\partial t} + \nabla \cdot (\mathbf{U} P_{Y\xi}) + \frac{\partial W_I P_{Y\xi}}{\partial y_I} + \frac{\partial S_I P_{Y\xi}}{\partial y_I} + \frac{\partial A_k P_{Y\xi}}{\partial \xi_k} - \frac{\partial^2 B_{kl} P_{Y\xi}}{\partial \xi_k \partial \xi_l} = D \nabla^2 P_{Y\xi} \quad (7)$$

for the joint PDF  $P_{Y\xi} = P_{Y\xi}(\mathbf{y}, \boldsymbol{\xi}; \mathbf{x}, t)$ , where the diffusion coefficient in the space of reference variables  $B_{kl} = b_{ki} b_{il} / 2$  is introduced. In conventional mixing models the mixing operator,

$$S_I = \mathbb{S}(y_I, [P_Y(y)]; \mathbf{x}, t), \quad (8)$$

depends on the current value of reactive scalars and is a functional of the local shape of the joint scalar PDF,

$$P_Y(\mathbf{y}; \mathbf{x}, t) = \int_{\infty} P_{Y\xi}(\mathbf{y}, \boldsymbol{\xi}; \mathbf{x}, t) d\boldsymbol{\xi}, \quad (9)$$

and weakly depends on  $\mathbf{x}$  and  $t$ .

The exact form of the functional depends on the mixing model. For example, Equation (8) is specifically for IEM and Curl's models. The mixing operator depends (explicitly but weakly) on  $\mathbf{x}$  and  $t$  due to changes in the characteristic mixing time from point to point.

The equation for the modelled joint scalar PDF is easily obtained by integrating Equation (7) over all reference variables resulting in equation,

$$\frac{\partial P_Y}{\partial t} + \nabla \cdot (\mathbf{U}_Y P_Y) + \frac{\partial W_I P_Y}{\partial y_I} + \frac{\partial (S_I)_Y P_Y}{\partial y_I} = D \nabla^2 P_Y, \quad (10)$$

that must be consistent with Equation (1) to produce a valid model.  $\mathbf{U}$  is a model for the velocity,  $\mathbf{u}$ , and here we introduce the conditional expectation of

the velocity,

$$\begin{aligned} \mathbf{U}_Y(\mathbf{y}; \mathbf{x}, t) &= \frac{\int_{\infty} \mathbf{U}(\boldsymbol{\xi}; \mathbf{x}, t) P_{Y\xi}(\mathbf{y}, \boldsymbol{\xi}; \mathbf{x}, t) d\boldsymbol{\xi}}{P_Y(\mathbf{y}; \mathbf{x}, t)} \\ &= \langle \mathbf{U}^* | \mathbf{Y}^* = \mathbf{y}, \mathbf{x}^* = \mathbf{x}, t \rangle \cong \mathbf{u}_Y(\mathbf{y}; \mathbf{x}, t). \end{aligned} \quad (11)$$

The last equality in this equation indicates that  $\mathbf{U}_Y$  is the model for  $\mathbf{u}_Y$ . The mixing operator,

$$(S_I)_Y = \frac{\int_{\infty} S_I P_{Y\xi}(\mathbf{y}, \boldsymbol{\xi}; \mathbf{x}, t) d\boldsymbol{\xi}}{P_Y(\mathbf{y}; \mathbf{x}, t)} = \langle S_I^* | \mathbf{Y}^* = \mathbf{y}, \mathbf{x}^* = \mathbf{x}, t \rangle, \quad (12)$$

is not affected by the integration over the reference variables in Equation (12) and  $(S_I)_Y = S_I$  since  $S_I$  specified by (8) does not depend on  $\boldsymbol{\xi}$ . The principal condition for consistency of the model (10) and the PDF Equation (1) is adequate modelling of dissipation by the mixing operator implying

$$(S_I)_Y P_Y = \mathbb{S}(y_I, [P_Y(y)]) P_Y \cong \frac{\partial N_{IJ} P_Y}{\partial y_J}. \quad (13)$$

Integration of this equation over all  $\mathbf{y}$  results in the following principal constraint

$$\langle S_I^* | \mathbf{x}^* = \mathbf{x}, t \rangle = \int_{\infty} \mathbb{S}(y_I, [P_Y(y)]) P_Y d\mathbf{y} = 0 \quad (14)$$

since the right-hand side of Equation (14) is nullified after integration due to  $P_Y \rightarrow 0$  as  $|\mathbf{y}| \rightarrow \infty$ . Integration of Equation (10) over all  $\mathbf{y}$  after multiplying this equation by  $y_I$ , indicates that any consistent mixing operator  $\mathbb{S}$  constrained by Equation (14) can affect the variance of  $Y_I$  but preserves the mean values  $\langle Y_I \rangle$ . This requires mixing to be performed locally in the physical space  $\mathbf{x}$ . We note that consistency of modelling is necessary but not sufficient for good modelling of turbulent combustion — mixing should satisfy a number of additional

conditions [21].

### 2.3. Generalised MMC and its consistency with the PDF equation

In the context of generalised MMC, a set of  $n_c$  conditioning variables  $\eta_1, \dots, \eta_{n_c}$  is defined as a subset of the reference variables, that is  $\boldsymbol{\eta} = \boldsymbol{\eta}(\boldsymbol{\xi})$ . The function  $\boldsymbol{\eta}(\boldsymbol{\xi})$  is degenerate as the dimension of  $\boldsymbol{\eta}$  is smaller than the dimension of  $\boldsymbol{\xi}$  and conditioning on these variables is not equivalent. A non-degenerate replacement  $\boldsymbol{\eta}'(\boldsymbol{\eta})$  of conditioning variables represents an equivalent condition  $\langle\langle \cdot | \boldsymbol{\eta}'(\boldsymbol{\eta}) \rangle\rangle = \langle\langle \cdot | \boldsymbol{\eta} \rangle\rangle$ . From this perspective, any smooth and non-degenerate replacement of conditioning variables does not alter the model. This statement is valid for a case of infinite resolution but, in practical simulations, the characteristic mixing distance is always finite and rescaling of different directions affects the outcome of conditioning of the mixing operator.

Here, we assume for the sake of simplicity that the first  $n_c$  reference variables are the same as the conditioning variables

$$\eta_i = \xi_i, \quad i = 1, \dots, n_c \quad (15)$$

i.e. the set of reference variables is given by

$$\boldsymbol{\xi} = \{\eta_1, \dots, \eta_{n_c}, \xi_{n_c+1}, \dots, \xi_{n_r}\} = \left\{ \underbrace{\eta_1, \dots, \eta_{n_c}}_{\boldsymbol{\eta}}, \underbrace{\xi_1, \dots, \xi_{n_r-n_c}}_{\boldsymbol{\zeta}} \right\}$$

where the remaining reference variables  $\xi_{n_c+1}, \dots, \xi_{n_r}$  are denoted by  $\boldsymbol{\zeta}$ . There is no loss of generality in this assumption, as we can always replace (or renumber) the reference variables.

The MMC models do not change the mixing operator directly but only require that mixing is performed locally in physical space  $\mathbf{x}$  and in the space of conditioning variables  $\boldsymbol{\eta}$ . While this preserves the original features of the mixing

model (linearity, independence, etc.), the mixing model is significantly enhanced by enforcing localness. The MMC mixing operator  $S_I$  is now represented by

$$S_I = \mathbb{S}(y_I, [P_{Y|\eta}(y)]; \mathbf{x}, t) \quad (16)$$

In MMC,  $S_I$  is exactly the same functional of the conditional PDF  $P_{Y|\eta} = P_{Y\eta}/P_\eta$  as  $S_I$  is a functional of the PDF  $P_Y$  in conventional mixing models (8). The PDF of the conditioning variables  $\boldsymbol{\eta}$  is denoted by  $P_\eta = P_\eta(\boldsymbol{\eta}; \mathbf{x}, t)$ . We first examine if this change affects the consistency of the model and the PDF equation. Since the form of the functional does not change, we can substitute the function  $P_{Y|\eta}$  for the function  $P_Y$  in (13)

$$\mathbb{S}(y_I, [P_{Y|\eta}(y)])P_{Y|\eta} = \frac{\partial N_{IJ}^\circ P_{Y|\eta}}{\partial y_J}. \quad (17)$$

Here,  $N_{IJ}^\circ$  remains the same functional of the PDF but we use the "o" superscript to indicate that  $N_{IJ}^\circ$  no longer corresponds to  $N_{IJ}$  defined by (3) (at least because the conditional variables  $\eta_i$  implicitly enter Equation (17) as additional parameters). We note that with (17) instead of (13) the mixing operation satisfies the following constraint

$$\langle S_I^* | \boldsymbol{\eta}^* = \boldsymbol{\eta}, \mathbf{x}^* = \mathbf{x}, t \rangle = \int_{\infty} \mathbb{S}(y_I, [P_{Y|\eta}(y)])P_{Y|\eta} d\mathbf{y} = 0 \quad (18)$$

which is stronger than (14). Once again, the "asterisk" superscript indicates stochastic values of parameters and functions.

The modelling equation for  $P_Y$  is once again obtained by integration of (7) over all  $\boldsymbol{\xi}$  and is given by (10). For the mixing operator, we multiply (17) by

$P_\eta$  and obtain

$$(S_I)_Y P_Y = \int_{\infty} S_I P_{Y\eta} d\boldsymbol{\eta} = \int_{\infty} \mathbb{S}(y_I, [P_{Y|\eta}]) P_{Y\eta} d\boldsymbol{\eta} = \int_{\infty} \frac{\partial N_{IJ}^\circ P_{Y\eta}}{\partial y_J} d\boldsymbol{\eta} = \frac{\partial N_{IJ} P_Y}{\partial y_J} \quad (19)$$

where

$$N_{IJ} P_Y = \int_{\infty} N_{IJ}^\circ P_{Y\eta} d\boldsymbol{\eta} \quad (20)$$

is the MMC model for  $N_{IJ}$ . Note that, according to (19), the MMC mixing operation is still consistent with the dissipation term in the PDF equation.

This leads us to the following proposition:

**Proposition 1.** *MMC modelling is consistent: conditioning of the mixing operation on reference variables (which can represent any modelled quantities) does not alter the consistency of the mixing model with the PDF equation. Conditioning of the mixing operator preserves linearity and independence provided the original mixing model possesses these attributes.*

#### 2.4. The effect of conditioning on the mixing operator

As discussed in the previous section, consistency of MMC modelling is important but it does not tell us much about the actual effect of MMC conditioning. We may note that conditioning does not compromise linearity, independence and conservation of species *and* at the same time improves localness of mixing. The main effect of MMC on the mixing operation can be expressed in terms of the conditional quantity  $Q_I(\boldsymbol{\eta}; \mathbf{x}, t) = \langle Y_I^* | \boldsymbol{\eta}^* = \boldsymbol{\eta} \rangle$  whose equation is obtained after multiplying (7) by  $Y_I$  and integrating this equation over all  $\mathbf{y}$  and  $\boldsymbol{\zeta}$  yielding

$$\begin{aligned} \frac{\partial Q_I P_\eta}{\partial t} + \nabla \cdot (\langle \mathbf{U}^* Y_I^* \rangle_\eta P_\eta) + \frac{\partial \langle A_i^* Y_I^* \rangle_\eta P_\eta}{\partial \eta_i} - \frac{\partial^2 \langle B_{ij}^* Y_I^* \rangle_\eta P_\eta}{\partial \eta_i \partial \eta_j} \\ - D \nabla^2 (Q_I P_\eta) - \langle W_I^* \rangle_\eta P_\eta = \langle S_I^* \rangle_\eta P_\eta = 0 \end{aligned} \quad (21)$$

where  $\langle \dots \rangle_\eta$  denotes the conditional expectation  $\langle \dots | \boldsymbol{\eta}^* = \boldsymbol{\eta}, \mathbf{x}^* = \mathbf{x}, t \rangle$ . Here, we take into account that  $\langle S_I^* \rangle_\eta = 0$  in MMC mixing due to (18). This is not valid in conventional mixing, where  $\langle S_I^* \rangle = 0$  but  $\langle S_I^* \rangle_\eta \neq 0$  and hence, under the assumptions of a conventional mixing model, the term  $\langle S_I^* \rangle_\eta P_\eta$  would remain on the right-hand side of equation (21). Therefore, the model for  $Q_I$  does not depend on the mixing operator in MMC, while  $Q_I$  is directly affected by the mixing operator in conventional models. MMC simulates only fluctuations with respect to  $Q_I$ , which are called *minor fluctuations* (*i.e.* the minor fluctuations can affect  $Q_I$  only through non-linear source terms  $W_I$ ). The implication of this simple statement is profound and can be expressed by the following proposition:

**Proposition 2.** *MMC generalises the PDF approach by combining it with conditional combustion models based on the mixture fraction and other types of reference variables; the conditional expectations  $Q_I$  do not directly depend on mixing and are determined by the properties of the conditioning (reference) variables.*

This proposition indicates that MMC is a hybrid model or, in more accurate terms, a method for hybridisation of models that unifies conditional and PDF approaches. MMC involves enforcing conditional properties, which are determined by the properties of the reference variables, on a mixing operation but without corrupting the operator. This is considered in the following example.

The CMC model is an approximation for transport of reactive scalars in mixture fraction space, which is consistent with the theory of the inertial interval and has proven to be reasonably accurate in most conditions and is in theory not restricted to the cases where conditional variances of reactive scalars are small. However, practical application of first order CMC is generally confined to these cases, since evaluation of chemical source terms expressed as functions of conditional means becomes inaccurate for large conditional variance. This can be remedied to some extent by solving equations for conditional variances and covariances, but the system of second-order CMC equations quickly be-

comes cumbersome and intractable even with a moderate number of reactive scalars. In this case we would be better served by solving stochastic equations of the PDF models. There is, however, another problem — conventional PDF mixing models are generally not CMC-compliant. This indicates that the reactive scalars are transported in the mixture fraction space with violations of the relationships of the inertial interval, localness of the dissipative transport or independence of reactive scalars. Practically, this means that, at least in some cases where solutions are sensitive to transport in the mixture fraction space, such mixing models can produce inaccurate results. Can this situation be remedied? Yes, MMC mixing allows for alteration of the mixing model in a way that the resulting mixing model becomes CMC-compliant. This possibility of CMC-compliant mixing was demonstrated in the original MMC [22, 25], where conditional variables effectively represent the properties of the mixture fraction.

As mentioned previously the conditioning variables in MMC can represent various properties of turbulent flows (note that any physical stochastic process can be approximated by a Markov process of sufficiently high dimension). Other known choices found to improve the quality of mixing models are velocity components and shadow position variables [31]. The flamelet solutions, where reactive species are parameterised by two parameters — mixture fraction and scalar dissipation — indicate that the conditional variables representing scalar dissipation can be useful in MMC [41]. It was found, however, that introducing dissipation-like conditioning variables offers little improvement for MMC models [26]. Against our *a priori* expectations, DNS and models demonstrated a lack of correlation between reactive scalars and the dissipation [26]. The lack of correlations between reactive scalars and conditioning variables does not invalidate the MMC model but makes conditioning of mixing on dissipation practically useless, resulting in unnecessary computational expenses. While MMC

mixing is conventionally applied to particle methods, conditioning of mixing is also possible (at least in principle) for other implementations of PDF methods, such as stochastic fields [14]. In the case of stochastic fields, MMC mixing between the scalar fields becomes conditional on the local value of the reference fields.

### 2.5. Modelling micromixing and MMC

The physical process of diffusion of multiple scalars in turbulent flow is characterised by at least two main characteristic timescales. The first is the characteristic time for dissipation of scalar fluctuations  $\tau_d$ . While dissipation physically occurs at small scales, the dissipation rate is controlled by the large-scale transport. The dissipation time  $\tau_d$  is similar to the integral time scale and, at the leading order, does not depend on the Reynolds number. All mixing models incorporate the time  $\tau_d$  and matching the overall dissipation rate is considered to be the key constraint imposed on all mixing models. The second timescale is the characteristic time for generation of conditional fluctuations  $\tau_g$ . From a theoretical perspective, this time is linked to the characteristic correlation time of the scalar dissipation, which is controlled by the processes in the inertial interval of turbulence. Practically, the generation time  $\tau_g$  is significantly smaller than  $\tau_d$  but noticeably larger than the time scale of the smallest fluctuations  $\tau_k$  (i.e. the Kolmogorov time scale) [23]. The generation time  $\tau_g$  can depend on the Reynolds number, although this dependence is weaker than that of  $\tau_k$ . The generation time becomes irrelevant when dissipation of a single scalar or several linearly dependent scalars are considered. However, in turbulent combustion, the time  $\tau_g$  controls generation of conditional fluctuations and extinction. In more complex combustion cases, where reaction rates are relatively slow, it is important that mixing models match not only  $\tau_d$  but also  $\tau_g$ .

The term *micromixing* is often used as a synonym for "mixing" emphasising that, physically, mixing occurs at small scales [9]. It seems, however that the use of *micromixing modelling* can be confusing in many cases as mixing models are introduced to match only the dissipation time  $\tau_d$ , which is a macro rather than a micro-parameter. The term *micromixing modelling* seems to be justified only when the mixing operation is introduced to model not only the large-scale dissipation rate but also at least some more refined properties of mixing controlled by smaller scales. Hence, our interpretation of modelling of *micromixing* is aimed at matching at least the two time scales  $\tau_d$  and  $\tau_g$ . It should be noted that *micromixing modelling* represents a goal and not the result: as any other mixing model, a *micromixing model* can be good or bad.

Most conventional mixing models match only one characteristic time — the dissipation time  $\tau_d$ . In this case, the dissipation time of the mixing operator  $\tau_S$  is linked to the dissipation macroscales:  $\tau_S \sim \tau_d$ . The MMC models are aimed at matching both the dissipation time and the conditional generation time (i.e. the level of conditional fluctuations) [23]. Theoretical estimates indicate that in this case  $\tau_S \sim (\tau_d \tau_g)^{1/2}$  [42] which is significantly smaller than  $\tau_d$ . The fluctuations with respect to conditional means, which are directly treated by the mixing operator emulate micromixing while the larger scales are controlled by the MMC reference variables. In MMC, the timescale  $\tau_S$  is called the micro (or minor) dissipation time to distinguish it from the conventional macro (or major) dissipation time  $\tau_d$ . Practically, in many MMC models the parameter  $\Lambda = \tau_S/\tau_d$ , which is known as a localness parameter, is noticeably smaller than unity. In the MMC regime, large-scale transport is mostly controlled by the reference variables matching the dissipation time  $\tau_d$ . This understanding of micromixing can be summarised by the following proposition:

**Proposition 3.** *Micromixing models differ from conventional mixing models by matching not only the macro-dissipation time but also at least some of the*

*more refined characteristics of turbulent mixing at smaller scales. MMC is an example of micromixing model in accordance with this definition.*

MMC models are aimed at modelling micromixing and typically use  $\Lambda$  that is noticeably less than unity. In general, MMC has two main effects: 1) better simulation of mixing due to localisation; and 2) modelling of micromixing. The IECM (interaction with conditional mean [43]), which is the velocity conditioned version of IEM improves the quality of simulation of mixing (as compared to IEM) but cannot model micromixing as we understand it here since the minor fluctuations in IECM are constrained by macroscopic transport properties. Hence, IECM is not a (true) MMC model. It needs to be stated that the possibility of modelling micromixing is not limited to MMC models. For example, EMST [21] can be modified to produce different generation times  $\tau_g$  [23].

### **3. Sparse and MMC modelling in the the LES context**

Our consideration of the previous section remains valid for LES conditions but instead of ensemble averaging, the average  $\langle \dots \rangle$  should be understood as LES filtering [8]. Hence, the MMC method remains consistent with the FDF transport equation. There are, however, a number of features that are specific to LES conditions. These features are discussed below. A large part of this section is dedicated to a simple explanation of sparse-Lagrangian methods. While from a theoretical perspective the sparse methods represent a concept independent of MMC, practical success of sparse methods in the dramatic reduction of computational cost of LES-FDF simulations is linked to using MMC. These simulations consist of an Eulerian LES for the simulation of velocity, pressure, and reference mixture fraction and a Lagrangian formulation of the FDF for the simulation of the reactive composition field.

### 3.1. What are the sparse methods?

The sparse models, which have been conceived and deployed in recent years are characterised by a relatively the small number of Lagrangian particles used in simulations. In FDF methods, the chemical reaction rates are evaluated only on the Lagrangian particles and this evaluation dominates the computational cost of the simulations, especially when the number of reactive species is large. A thousandfold reduction in particle numbers, which is accompanied by a similar reduction of the computational cost, has been demonstrated with sparse methods [34, 36, 44]. While the possibility of reducing computational cost by deploying fewer particles is obvious, the conceptual possibility of a substantial reduction in the number of particles is not trivial, requiring alternative understanding of principles used in FDF simulations. Thus, the reduction of particle numbers is not the key idea behind the sparse methods but only a consequence of a new interpretation of Lagrangian PDF modelling. In conventional approaches, which we call *intensive*, the target is to reproduce the joint composition PDF in every Eulerian cell. Hence, in intensive methods: 1) mixing is confined to be between particles within the same Eulerian cells; and 2) many particles per cell are required. In intensive methods, the characteristic mixing scale  $\Delta_m$ , which characterises the average distance between particles subject to mixing, coincides with the size of the Eulerian grid  $\Delta_g$ .

In *sparse* methods, the particles are not confined to representing an FDF within Eulerian cells, but are allowed to mix across Eulerian cells, while  $\Delta_m$ , which represents the characteristic distance associated with this mixing, can be greater than  $\Delta_g$ . The sparse methods consider every Lagrangian particle as a sample of scalar composition at its location while mixing between particles is not restricted by the cell boundaries. This introduces a more efficient mixing since two close particles separated by Eulerian grid boundaries are allowed to be mixed

in sparse but not in intensive simulations. Effectively, sparse FDF simulations use two grids: a conventional Eulerian grid, which is used to represent velocity, pressure and some scalar fields, and a moving Lagrangian grid, which is used to represent the reactive scalars. The Lagrangian and Eulerian representations of physical quantities are similar but not exactly the same (for example, the Eulerian and Lagrangian representations of the mixture fraction have a degree of stochastic variations with respect to each other). These stochastic variations of the Lagrangian representations are controlled to represent subgrid fluctuations of the scalar fields [45].

In general, sparse FDF simulations are characterised by four characteristic scales: the Eulerian filtering scale  $\Delta_E$ , the size of the Eulerian grid  $\Delta_g$ , the Lagrangian filtering scale  $\Delta_L$  and the distance between Lagrangian particles  $\Delta_p$ . While scales do not necessarily coincide that obvious constraints that  $\Delta_E \geq \Delta_g$  and  $\Delta_L \geq \Delta_p$ , which are discussed below. In conventional LES, the filtering scale  $\Delta_E$  cannot be smaller than the grid size  $\Delta_g$ , which restricts the resolution of the evaluated fields. Methodologically, we might wish to distinguish modelling and numerical errors. The numerical errors can be made negligible by selecting  $\Delta_g \ll \Delta_E$ , although this causes a substantial increase of computational expenses. Practically, if we have a refined grid with small  $\Delta_g$ , the corresponding reduction of  $\Delta_E$  to  $\Delta_E \approx \Delta_g$  would ensure a better quality simulations with a wider range of resolved scales. Thus, most practical simulations are conducted under conditions  $\Delta_E \approx \Delta_g$  while the case  $\Delta_g \ll \Delta_E$  is deployed only for analysis of methodological issues.

This consideration is mirrored on the Lagrangian side. The analysis of mixing [46] indicates that, in sparse conditions, the characteristic Lagrangian filtering scale  $\Delta_L$  is connected to the characteristic mixing scale  $\Delta_L \approx \Delta_m$ , since mixing induces numerical diffusion that preforms filtering of the scalar

fields. Obviously, since the mixing distance  $\Delta_m$  is not the characteristic distance between the closest particles  $\Delta_p$  but the characteristic distance between the particles that are allowed to be mixed,  $\Delta_m$  must be the same or larger than characteristic distance between the particles:  $\Delta_m \geq \Delta_p$ . Theoretically, as in the case of Eulerian grid, we can have a very large number of particles that ensures that  $\Delta_p \ll \Delta_m \approx \Delta_L$ , which, as discussed further in the next subsection, would reduce the stochastic errors in instantaneous representations of the reactive scalar FDF. As in the case of the Eulerian grid, this is computationally expensive but does not increase the resolution and can be useful for restrictive methodological analysis. In practical simulations, modelling errors can be decreased by reducing  $\Delta_m$  as much as possible for given computational resources so that  $\Delta_m \approx \Delta_p$ .

The above considerations can be summarised by the following proposition:

**Proposition 4.** *Unlike conventional intensive FDF methods, sparse simulations are not aimed at reproducing complete joint FDFs of reactive scalars locally and instantaneously within each Eulerian cell but, nevertheless, still account for subgrid fluctuations of the reactive scalars. In sparse simulations, mixing is not restricted by or connected to the Eulerian grid.*

There is another constraint that needs to be mentioned here:  $\Delta_L \geq \Delta_E$ . Indeed since Eulerian subfilter scales are not resolved for the velocity field, these scales cannot be resolved for the scalar fields. While sparse mixing algorithms (which are based on distance between particles irrespective of the cell boundaries) can be applied for the case of many particles per Eulerian cell, this would not lead to reduction of  $\Delta_L$  below  $\Delta_E$  even if  $\Delta_m = \Delta_p \ll \Delta_g$  since transport processes at the Eulerian subfilter scales are modelled by particle diffusion and the resolution of the velocity field limits the maximum possible resolution of the scalar fields. In principle MMC modelling can be performed within each cell, further improving the localisation of mixing but this is not considered here. The influence of the number of particles per cell on simulations is considered further

in the next subsection.

### 3.2. Reducing the number of particles

First, we consider the case of many Lagrangian particles per Eulerian cell (i.e.  $\Delta_p \ll \Delta_g$ ). The conventional algorithm, which is here called *intensive*, implies that any two or more particles within the same cell can be mixed, that is  $\Delta_m \approx \Delta_E$ . The *sparse* algorithm, however, traces particle positions within each cell and allows for mixing of closest particles, whether these particles are currently located within the same cell or not (hence  $\Delta_m = \Delta_p$ ). Although  $\Delta_p \ll \Delta_g$ , the filtering scales  $\Delta_L \approx \Delta_E$  are practically the same for both algorithms, intensive and sparse, due to the effect of subgrid diffusion modelled by the random motion of particles. For the case of many Lagrangian particles per Eulerian cell, the intensive and sparse algorithms can be expected to produce very similar results.

The number of particles per cell can be reduced. In the case of intensive simulations, this reduction is constrained by the need of having at least several particles per cell since, otherwise, mixing becomes impossible. The same constraint applies to the FDF methods using stochastic fields [14], which are also necessarily intensive as they must involve a sufficient number of stochastic fields. This constraint, however, does not apply to sparse simulations, where particles can be found in the neighbouring cells to form mixing groups. Initially, when  $\Delta_p \ll \Delta_g$ , the reduction of the number of particle per cell does not change the filtering scales  $\Delta_L \approx \Delta_E$ ; the main effect of the reduction is the increase of stochastic errors in evaluation of average properties within each cell, which, at the leading order, does not change the model. (Strictly speaking mixing models are not fully invariant with respect to the number of particles and reduction of particles may lead to loss of stochastic independence of the particles or to increased probability of extinction events [47]; simulations often indicate existence

of a degree of dependence of the results on the particle numbers [48]).

The sparse mixing algorithm can easily reach the characteristic case of having approximately one Lagrangian particle per Eulerian cell, where all major scales coincide  $\Delta_p \approx \Delta_m \approx \Delta_L \approx \Delta_E \approx \Delta_g$ . Up to this case, the main effect of a reduction in the number of particles is not a significant change of the Lagrangian filtering scale but an increase of stochastic errors in the FDF representation and a reduction in computational cost. Any further reduction of the number of particles must increase the distances  $\Delta_p$ ,  $\Delta_m$  and  $\Delta_L$  above  $\Delta_g$ . This changes the model by reducing localness of mixing. There is, however, a potential benefit in having  $\Delta_m \approx \Delta_L > \Delta_E \approx \Delta_g$  due to a further reduction of the computational cost associated with evaluating chemical species, which can be particularly high for realistic kinetics.

### 3.3. Stochastic and biased errors in sparse simulations

The main implication of the reduction of the number of particles per cell is the increase in the stochastic error for any average (filtered) quantity determined locally and instantaneously. This, however, does not necessarily mean that reduction in the number of particles introduces additional bias into simulations. In fact, if the mixing distances are kept the same, reducing the number of particles does not change the model at the leading order. However, the characteristic filtering distance  $\Delta_L$  cannot be smaller than the characteristic mixing distance  $\Delta_m$ , which in its turn cannot be smaller than the distance between the particles  $\Delta_p$ . Hence, a reduction of the number of Lagrangian particles below the number of Eulerian grid points increases  $\Delta_L \approx \Delta_m$  over  $\Delta_g$  and changes the model due to the bias associated with diffusion induced by mixing [35, 46, 47].

Numerical convergence in LES is conventionally investigated by reducing grid size  $\Delta_g$  while keeping the Eulerian filtering scale  $\Delta_E$  the same (reducing  $\Delta_E$  consistently with  $\Delta_g$  would change the model). In the same way, numerical

convergence of PDF/FDF methods can be tested by increasing the number of particles but keeping the characteristic mixing distances the same. In conventional intensive methods, the mixing distance  $\Delta_m$  is linked to  $\Delta_g$  and does not change with increasing the number of particles, and a similar effect of fixing mixing distances can be achieved in sparse simulations. As in LES convergence tests, this requires reducing  $\Delta_p$  while keeping  $\Delta_L = \Delta_m$  the same, which corresponds to abandoning mixing of the closest particles. Theoretically, the number of particles can be arbitrarily large while the model still remains sparse [46], but practically the number of particles is limited by computational resources. We note that convergence tests are useful only from a methodological perspective but are inefficient from a practical perspective as they do not represent optimal simulations (i.e. highest quality and resolution at minimal computational cost). Most LES studies are conducted with the filter size being fixed to the grid size. Results of a numerical convergence study for sparse-Lagrangian FDF simulation are presented in Section 4.1.

Practical sparse simulations have to tolerate significant stochastic errors, which must not be confused with other, regular errors present in the simulations. Imagine particles distributed as one (or very few) particles per cell with the values of species generated randomly according to an absolutely correct FDF. In this case and assuming steady-state flow, we can easily evaluate the correct FDF over larger volumes or longer periods of time, thereby reducing stochastic error, but we cannot determine these FDFs locally and instantaneously [49]. In combustion applications, when the overall production of pollutants is of interest, we might not need detailed FDF distribution of all species in every cell at every time moment. In this case reducing the number of particles is a good idea — this is exactly the idea that is implemented in sparse methods. There are, however, more subtle problems in such reduction that need to be considered.

The main problem comes from the fact that combustion, which is governed by highly non-linear kinetic equations, can be extinguished. If there are many particles in every cell, a particle might occasionally acquire a low temperature sufficient for extinction but this does not cause global extinction due to immediate mixing with other particles which are burning. If, however, there are very few particles in the cell and one of the particles occasionally acquires a low temperature, then the whole cell can become extinct after mixing. Extinction in one cell can propagate into other cells causing global extinction. A low number of particles can increase the statistical significance of rare events. This effect is exacerbated by the trend of the Curl's and IEM models to over-produce extinctions due to non-local mixing. In sparse conditions, mixing is often performed at larger distances  $\Delta_m > \Delta_g$ , which reduces localness and also stimulates extinctions. Hence, reducing the number of particles in sparse conditions is not likely to work when mixing is modelled by conventional models and this expectation corresponds to our experience (here we refer only to the IEM and Curl's models — it is quite possible that EMST [21], which has good localisation, can work under sparse conditions but this has not been tested yet). Practically, sparse methods require modelling of micromixing and the correction of conventional mixing models by MMC.

#### *3.4. MMC in LES conditions*

The LES-MMC model allows for different interpretations. For example, one might see the whole Eulerian LES as producing suitable conditioning variables for generalised MMC. The simplest explanation of the LES-MMC approach is related to flamelet-type considerations. The key assumption of the flamelet model [5] is a strong dependence of the reactive scalars on the mixture fraction, which is expressed mathematically by asymptotic stretching of the variable associated with the mixture fraction. In doing this asymptotic stretching, the conventional

derivation of the flamelet model discriminates physical coordinates and, thus, is not fully coordinate-invariant. The sparse-Lagrangian MMC approach in LES conditions for non-premixed flames introduces a metric that defines the effective distance between particles A and B by

$$d_{\text{AB}}^2 = \sum_{i=1}^3 \left( \frac{\sqrt{3} x_i^{(\text{A})} - x_i^{(\text{B})}}{r_m} \right)^2 + \left( \frac{f^{(\text{A})} - f^{(\text{B})}}{f_m} \right)^2 \quad (22)$$

where  $f^{(\text{A})}$  is the Eulerian value of the reference mixture fraction, evaluated at the location of particle A,  $x_1^{(\text{A})}$ ,  $x_2^{(\text{A})}$  and  $x_3^{(\text{A})}$  are the particle's physical coordinates and  $r_m$  and  $f_m$  are parameters whose ratio  $f_m/r_m$  controls the degree of MMC localisation. This ratio is linked to the previously used localisation parameter of  $\lambda$  [34, 44], with  $f_m/r_m \approx L_x \lambda / L_f$  where  $L_x$  and  $L_f$  are characteristic physical and reference scales set to the jet nozzle radius and unity, respectively.

Here,  $f_m$  is treated as a free parameter while the choice of  $r_m$  is constrained by theoretical considerations and discussed in previous work [49]. If  $f_m$  is large (more accurately  $f_m/r_m \rightarrow \infty$ ), then equation (22) defines the conventional distance normalised by  $r_m$ . If  $f_m$  is sufficiently small, then the mixture fraction term becomes very significant.

Conceptually, this corresponds to the coordinate-invariant version of the flamelet model [50] which deploys a flamelet transformation without discriminating the physical coordinates, which is the same as the conventional flamelet model at the leading order but possesses additional useful properties that are important for our consideration. This procedure also corresponds to MMC conditioning, assuming that the MMC reference variables are represented by  $f^{(\dots)}$ . The Eulerian mixture fraction  $f$  should be distinguished from the Lagrangian mixture fraction, which is evaluated from the simulated reactive scalars  $Y_I^*$  — MMC models with mixture fraction conditioning have two mixture fractions. Let us consider in detail how the new definition of the distance, defined in

Equation (22) affects mixing.

If simulations are conducted in multiple dimensions, the positions of different particles never coincide and mixing has to be performed with some finite physical distance between particles. This results in additional diffusion induced by the mixing process [45, 47]. This diffusion performs filtering at distances  $\Delta_m \approx \Delta_L$  [34]. Hence, only particles which have minimal distance between them are allowed to be mixed. Consider Curl's mixing shown for the particles shown in Figure 2 of several notional particles separated by some physical distance in a mixture fraction field. If the conventional definition of distance (i.e.  $f_m/r_m = \infty$ ) is adopted, particle A is to be mixed with particle B and this may cause an extinction, while strong dependence of reactive scalars on  $f$  results in excessive numerical fluxes across the surface of  $f = \text{const}$  due to a lack of localness in this direction, as illustrated in Figure 2. This problem could be addressed by increasing the number of particles and reducing  $\Delta_L$ , but this path would be computationally expensive and MMC offers an alternative. If  $f_m$  is sufficiently small, then particle C is closest to the particle A according to the new definition of distance (Equation (22)). This improves modelling by localising mixing in the mixture fraction space, reducing excessive numerical fluxes across the surface of  $f = \text{const}$  and, thus avoiding spurious extinctions.

The new definition of mixing also has a side-effect; the distance between particles along the surfaces of  $f = \text{const}$  are increased. This results in increased numerical diffusion along these surfaces. In most cases, this increase is not crucial, since the evolution of conditional expectation  $Q_I = \langle Y_I | f \rangle$  is not sensitive to diffusional fluxes along the surfaces of  $f = \text{const}$  as shown for the coordinate-invariant version of the flamelet model [50] (provided, of course, that these fluxes do not become excessively large). Note that the MMC approach is aimed at modelling both the conditional expectation  $Q$  and fluctuations with

respect to  $Q$ .

It must be noted that the validity of the flamelet model is not needed and is not assumed here or anywhere in MMC while the reactive scalars have significant fluctuations with respect to any type of flamelet or equilibrium solutions. It is important, however, that the reactive scalars in non-premixed cases have a significant correlation with the mixture fraction, otherwise conditioning on mixture fraction is formally correct but is much less useful from a practical perspective. This does not exclude the use of reference variables besides mixture fraction. We thus do not expect that the dramatic thousandfold reduction of the computational cost (which has been achieved in sparse MMC simulations) is possible for complex flows, where the correlation between the mixture fraction and the reactive scalars is less significant. With respect to LES of non-premixed combustion, this correlation is exploited to our advantage as simpler cases allow us to use more economical setups for LES with MMC using relatively few particles, but we note that more complex cases may demand an increased number of particles. The hybrid nature of the MMC approach is an opportunity to have a single universal model that can perform both economical simulations of relatively simple cases and expensive simulations of more complex cases and leads to our fifth and final proposition:

**Proposition 5.** *The key factors that allow for a reduction of computational cost in sparse-Lagrangian large eddy simulations are the conceptual flexibility of sparse models, the incorporation of a physical understanding of turbulent combustion processes and the conditioning of mixing into PDF modelling achieved by MMC hybridisation of the model. This approach is universal, in that it can work under more sparse and more intensive conditions (without changing the algorithm) as demanded by the complexity of the flame case.*

#### 4. Simulation results and evaluation of MMC parameters

We illustrate the performance of the generalised MMC model under sparse conditions for three flame cases. In each case, MMC conditioning is enforced on

Modified Curl’s model [19, 20]. Previously published results from an idealised jet flame with a one-step flamesheet reaction and a thin reaction zone [8] and the simulations of the Sandia D-F flame series [38] are discussed in comparison with new sparse simulations of the Cabra lifted hydrogen flame [39]. For these cases, we examine the choice of the sparse MMC parameter  $f_m$ , which determines the characteristic distance between particles in the reference space in (22) and is the key MMC parameter determining the degree of localness and controlling conditional fluctuations (the details of selection of the parameters can be found in other publications [36, 49]).

In line with our five propositions, we demonstrate the ability of sparse methods to enforce conditional moments,  $Q_I$ , and control conditional fluctuations despite a relatively low number of particles and to balance computational cost and level of detail in the predictions. Indeed, all three cases are simulated on single workstations, with the relatively low computational cost enabling the use of detailed kinetics for the Sandia and Cabra flames. The simulations of the idealised jet flame and the Sandia series were performed using the Flowsi LES code initially developed by Kempf et al. [51] which was modified to incorporate the hybrid FDF-MMC model. For these two flames, we report some new results in addition to those reported previously [36, 49]. The Cabra lifted flame was tested on the OpenFOAM platform with the use of a newer FDF-MMC code, *mmcFOAM*, which can handle both sparse and intensive cases and has been developed through cooperation of several universities (The University of Sydney, The University of Queensland, Bundeswehr University at Munich, Stuttgart University and others).

#### 4.1. One-step flamesheet reaction

This case enforces conditions similar to those used in Colucci et al. [8], where fuel and oxidiser react rapidly in a one-step irreversible reaction to form the

product. The thinness of the reaction zone for this idealised flame sheet makes it a difficult test case for mixing models. Non-local mixing models, such as IEM and Curl’s, cannot reproduce the solution, while EMST performs quite well in this case [8]. Conceptually, sparse conditions decrease localness and exacerbate extinctions but the enforcement of localised mixing by MMC is shown to improve simulations even under sparse conditions. The details of these MMC simulations are given in [49].

Figure 3 shows scatter plots of the burning index versus instantaneous FDF mixture fraction field ( $z$ ) for several particle densities - an intensive case of 20 Lagrangian particles per Eulerian cell (denoted as 20L/1E), a case of intermediate particle density with 1L/1E and a sparse case of 1L/8E. We use the MC mixing model without localisation (corresponding to an infinite  $f_m$ ) and MMC-MC mixing model with two localisation values  $f_m$  of 0.04 and 0.06.

The reactive scalar is strongly dependent on localisation, as shown in Figure 3. The intensive case with no conditioning produces more conditional fluctuations and has the greatest departure from the equilibrium or flamelet solution of all the cases shown. Enforcing localness on the mixing operator via selection of a small, finite value of  $f_m$  consistently reduces these fluctuations. Conditional fluctuations are strongly dependent on the degree of localisation in the reference space, with a smaller value of  $f_m$  leading to fewer departures from the equilibrium composition and to a more accurate prediction for this case. This level of control over the fluctuations does not appear possible with the non-local mixing model. The value  $f_m$  of 0.04 produces results closest to the equilibrium condition out of the cases presented here. Our previous work [49] indicates that  $f_m$  of 0.02 reduces scattering even further. The values  $f_m$  from the range [0.02,0.04] tends to produce reasonable results for this case.

The effect of particle density or sparseness on localisation is evident in Fig-

ure 3. The decrease of the number of particles from 20L/1E to 1L/1E and finally to 1L/8E for  $f_m$  of 0.04 progressively increases scattering. For this sparse case, more localised mixing with a lower  $f_m$  is necessary to offset the reduction in particles. Per our fifth proposition, MMC enables flexible use of the PDF method and allows for the possibility of reducing computational cost and/or increasing quality of simulations by assigning useful properties onto the PDF model.

Figure 1 illustrates a numerical convergence test conducted for the same case where three simulations with different particle number densities are considered. We first consider a single set of particles (1L/32E), and then double (1L/16E) and quadruple (1L/8E) the original number of particles. The algorithm for this convergence check must ensure that mixing distances remain the same, and this can be achieved in many different ways. We use a relatively simple algorithm, where particles are divided into two or four groups at random prior to the nearest-neighbourhood search, such that each group contains the same number of particles. Mixing couples are then determined within each group. This ensures that the mixing distances between particles of each group remain consistent and all three cases have a fixed degree of localisation. A trend of convergence is visible in Figure 1 with an increase in particle numbers. We note that increases in the number of particles are limited by computational cost, while increases in the number of particles without a corresponding improvement in resolution are mostly impractical. Further details on this test can be found in [52].

#### 4.2. Sandia Flames D, E and F

We now present results for the Sandia flame series, where the Reynolds number of a piloted methane jet injected into a co-flow increases progressively from flame D to F. Flame D has the lowest injection velocity and is the most stable and is easiest to simulate relative to the other cases. Conversely, flame

F is close to global extinction and is the most challenging case to simulate. Modelling of the Sandia flame series requires accurate simulation of conditional variances. The conventional models (Curl’s and IEM) tend to overestimate the level of conditional fluctuations, have difficulties in reproducing flame E and keeping flame F burning, while EMST can reproduce the series quite well, albeit with some underprediction of conditional fluctuations [7]. Generally, sparseness of simulations strongly exacerbates the extinction problem but, in combination with MMC, the sparse-Lagrangian model can predict the series reasonably well due to strong control over the level of conditional fluctuations [12, 36, 44].

Simulations with one Lagrangian particle per 27 Eulerian cells (1L/27E) are employed for flames D-F. The GRI-Mech 3.0 kinetic scheme [53] with 219 reaction steps and 34 species (NOx excluded) is applied to each particle. Further details on the setup of this case can be found in previous publications [12, 36, 44]. The dissipation of mixture fraction is well matched by the LES for each flame which permits the accurate prediction of the more refined flame characteristics, per our third proposition.

Figures 4 and 5 shows radial profiles of the steady-state mean and rms of the OH mass fraction. These unconditional profiles of OH and CO match reasonably well with experimental data. Enforcing MMC on the micromixing model permits control over conditional fluctuations and variance. First and second unconditional and conditional moments of the reactive species are of comparable accuracy to previously published intensive Lagrangian simulations using stochastic fields by Jones and Prasad [14]. Most importantly, the results for the Sandia flames demonstrate that a single value of  $f_m = 0.03$  correctly predicts the trend of increasing local extinction with progressively increasing jet velocity. This value of  $f_m$  is consistent with the values used for the flamesheet case in the previous subsection of  $f_m$  (0.02-0.04). We note that an increase to

$f_m = 0.035$  improves the fluctuations for flame D without resulting in changes to the mean but causes global extinction in flame F [52].

#### 4.3. Cabra Lifted Flame

The Cabra hydrogen lifted flame [39] exhibits great sensitivity to physical conditions of the case. For example, a study replicating the original experimental conditions yields a lift-off height of approximately 30 diameters compared to the original value of 10 [54]. In another parametric study, a reduction in the temperature of the vitiated coflow from the experimental value of 1045 K to 1020 K results in lift-off height increasing from approximately 10 to 20 diameters [55]. From a mathematical perspective, this problem is ill-posed. In the development of the flame, convective processes and ignition plays a key role, while the quality of the mixing model has been found to be of less importance [56]. Generally, the *a priori* expectation is that more intensive simulations might be necessary to reproduce this flame. Here, we report the results of sparse simulations that nevertheless model this flame quite well. The lift-off height, however, appears to be sensitive to the localisation parameter.

This lifted flame is formed by a cold fuel jet with a bulk velocity of 107 m/s at 305 K issuing into a hot co-flowing oxidiser moving at 3.5 m/s at 1045 K. The central nozzle of the burner has a diameter of  $d = 4.57$  mm and extends 70 mm above a perforated base plate, which induces the vitiated co-flow. The fuel composition by volume is 25%  $H_2$  and 75%  $N_2$ . The stoichiometric mixture fraction is  $z_{st} = 0.47$ .

The LES problem is formulated for a 3D polar coordinate system at the central nozzle transitioning radially to a Cartesian coordinate system. There are 640 equally spaced cells in the axial direction, 8 and 24 cells in the radial direction of the core and co-flow respectively, and 32 cells in the azimuthal directions. The number of Eulerian cells totals to approximately 655,000 with

the smallest cells at the axis measuring  $0.3\text{mm} \times 0.4\text{mm} \times \pi/32$  radians. The domain is  $30d \times 30d \times 55d$ , where  $d$  is nozzle diameter as noted above.

Reaction source terms are evaluated from the chemical kinetic scheme of Mueller [57] containing nine species and 21 reactions. One particle per 32 Eulerian cells (1L/32E) is employed in all the lifted flame simulations shown here.

Based on the prescribed inlet jet velocity of 107 m/s and the axial domain length of approximately 250 mm, a single flow-through time is 2.3 ms. Each simulation is run for a minimum of five flowthrough times prior to any data sampling. Following this, data is sampled over approximately five flowthrough times from the time at which flame stabilisation is observed. Results are recorded and sampled every 500 time steps typically for 30000 time steps, with sampling and averaging performed over approximately 60 time steps.

We present axial profiles of the experimental and Lagrangian and Eulerian simulated mean and rms mixture fraction for a simulation case with  $f_m$  of 0.08, which yields the closest match to the experimental result of mixture fraction in Figure 6. Although slightly under-predicted, the mean Lagrangian results are noticeably better than the Eulerian mixture fraction predictions which are overly diffusive. Per our proposition that mixing is conditioned purely on the reference variable, the Lagrangian and Eulerian mixture fraction fields are topologically similar, reinforcing the role of the Eulerian mixture fraction as this reference variable. The improved accuracy of the sparse-Lagrangian relative to the Eulerian results is attributed to the mixing timescale model which is valid in the inertial range,

$$\tau_S^{A,B} = C_L^{-1} \frac{\widetilde{f_L'^2}}{\widetilde{f_E'^2}} \tau_d, \quad (23)$$

where  $\widetilde{f_E'^2}$  is the subfilter variance of reference mixture fraction at the Eulerian filtering scale  $\Delta_E$  and  $\widetilde{f_L'^2}$  is variance of particle mixture fraction at the

mixing scale  $\Delta_m$ . The parameter  $C_L$  can also be tuned to control conditional variances but is fixed here. We note here that the minor dissipation time  $\tau_S$  and the major dissipation time  $\tau_d$ , where  $\Lambda = \tau_S/\tau_d$  (or the ratio of relative importance of the chemical processes to the mixing processes), are linked by a constant  $C_L$  in Equation (23). Equation (23) adjusts the particle mixing timescale so that the rate of decay of Lagrangian scalar variance matches that of the Eulerian LES while accounting for the increased length scale in the Lagrangian field  $\Delta_L$ .

The sparse-Lagrangian MMC model tends to over-predict the peak axial mixture fraction rms, which is typical for other FDF simulations. In comparison, the time-averaged reference mixture fraction RMS is generally in better agreement with experimental data. While lower Lagrangian mixture fraction RMS predictions are possible through the reduction of the micromixing timescale, numerical diffusion would likely result in more inaccurate predictions for the mean. In the presented simulation, the micromixing time constant was set to  $C_L = 1.25$ . This slightly higher value of  $C_L$  compared to the usual value of unity has the effect of reducing the mixing timescale  $\tau_S$  and decreasing the conditional fluctuations. The effect of  $C_L$  is relatively minor and  $C_L = 1$  is also suitable for these simulations. Figure 7 shows radial profiles of the steady state mean and RMS of the Lagrangian mixture fraction. We generally observe good agreement between the simulated and experimental means at all locations with slight over-prediction of the rms.

Axial profiles of experimental and unconditional Lagrangian mean and rms temperature are shown in Figure 8. The predictions are generally in very good agreement with experimental data, although mean and rms temperatures are slightly over-predicted up to 30d from the nozzle which can be associated with the early jet break up that is noticeable in the axial mixture fraction profile.

The OH radical, a product of chain initiation, is a good indicator of flame lift-off height. Using a threshold of  $Y_{OH}$  of  $2 \times 10^{-4}$  we predict lift-off to occur at  $9.4d$  from the inlet, relatively close to the experimental lift-off height of  $10d$ . Figure 9 shows steady-state mean radial profiles of OH at several axial locations. Mean OH is under-predicted at  $x/d = 11$ , indicating that the width of the inner jet core is over-predicted. The under-prediction of OH at this location can be attributable to the slight difference in the predicted lift-off height relative to experimental results. It is also worth noting that the particle mixture fraction predictions are accurate at this point. The accuracy of our results is comparable to the LES-CMC simulations by Navarro-Martinez and Kronenburg [58] which employ the detailed Yetter mechanism [59]. OH predictions appear more accurate in the intensive RANS-PDF calculations by Cao et al. [56] which employ 100 Lagrangian particles per cell with EMST as the mixing model and the detailed Li mechanism [60]. Steady-state conditional OH profiles shown in Figure 10 also compare reasonably well with experimental data. The stochastic error observed in this figure, which is also present in the OH profiles of the Sandia series in Figure 4, is attributed to the sparse distribution of particles in both cases.

It is possible to model the Cabra hydrogen flame with reasonable accuracy under sparse conditions, reinforcing propositions three, four and five. Conditioning mixing on the mixture fraction, as in the previous two cases, is necessary to predict the unconditional and conditional means and variances, and lift-off height. We note that increasing  $f_m$  reduces the role of MMC and in the limit, this corresponds to modified Curl’s model. We now examine the influence of  $f_m$  on the reactive field and lift-off height. Figure 11 shows lift-off height normalised by jet nozzle diameter versus  $f_m$ . We note that the simulation results for each case is sampled over the same period of time once stabilisation is ob-

served. There is a high degree of lift-off height sensitivity to  $f_m$ , with flame attachment to the nozzle occurring when  $f_m < 0.07$ . Lift-off height increases monotonically with  $f_m$  as the mixture fraction term in Equation (22) becomes less significant.

Figure 12 compares scatter plots of OH for two values of  $f_m$  with otherwise identical model parameters. Both sets are sampled at the same axial location over the full sampling times and are sufficiently far downstream of the stabilisation point. The case with a lower  $f_m$  (of lower lift-off height) has fewer conditional fluctuations and exhibits a more flamelet-like band compared to that with a higher  $f_m$  which has more fluctuations. These fluctuations are directly treated by the mixing operator to emulate micromixing, with larger scales being controlled by the mixture fraction.

Under these sparse conditions imposed for the lifted flame, we observe that mixing performed with reduced localness and corresponds to relatively large mixing distances  $\Delta_m$  reduces flame stability and can stimulate extinctions. It is conceivable that the occurrence of isolated turbulent events where the temperature (and corresponding scalars) of a small number of particles deviates sufficiently from the mean can propagate into other cells causing global extinction. These rare events are particularly important for very sparse simulations where each particle represents a significant mass of fluid. As long as the lift-off height is matched by selecting  $f_m$ , the simulation of reactive scalars is satisfactory despite a high degree of sparseness in the simulations.

The value  $f_m \approx 0.08$ , which ensures the best match with the experiments is noticeably higher than  $f_m \approx 0.03$  which was found to be a good choice for both the Sandia flames D-F series and for the one-step flamesheet case previously discussed. Reactive scalar predictions are strongly dependent  $f_m$ , with larger values causing departure from flamelet-like conditions and greater conditional

variance. It seems that highly sparse simulations are not particularly suitable for this lifted flame. The unusual value of  $f_m = 0.08$  is likely a reflection of this fact.

## 5. Conclusions

This work presents the current understanding and theory on the generalised Multiple Mapping Conditioning approach in its most simple and transparent form as opposed to a step-by-step historic development. MMC is viewed as a hybrid approach, which effectively blends PDF models with CMC, flamelet or other models that can be formulated in terms of conditional expectations. MMC essentially enforces the desired conditional properties on the mixing operation. This hybrid nature of MMC improves quality of simulations and allows for greater control in simulation of micromixing. The sparse approach represents an alternative interpretation of Lagrangian modelling that is not aimed at reproducing joint FDFs of reactive scalars within every Eulerian cell but, nevertheless, still fully account for subfilter fluctuations of reactive scalars. While, conceptually, the sparse approach is not necessarily linked to MMC, all highly sparse simulations have been performed with the assistance of MMC. Changing the mixing distances alters the model, although numerical convergence can be checked by increasing the particle number density and simultaneously preserving these characteristic mixing distances.

We present new sparse-Lagrangian MMC simulations of the Cabra lifted hydrogen flame – the case, which is mathematically ill-posed and especially difficult for sparse-Lagrangian MMC. The simulations are compared with sparse-Lagrangian MMC simulations of the idealised jet flame with one-step flamesheet reaction and the methane Sandia Flame series D-F. The MMC localisation parameter, which is a key parameter in MMC modelling of micromixing, is rep-

resented in sparse-Lagrangian MMC simulations by  $f_m$ . While the simulations of methane Sandia Flame series D-F and the idealised jet flame have consistent values of  $f_m \approx 0.03$ , the simulations of the Cabra lifted flame are less localised with  $f_m \approx 0.08$ . We believe that very sparse simulations are less suitable for highly sensitive lifted flames. Nonetheless, sparse-type algorithms and MMC are universal, in the sense that there is no need to alter the mixing algorithm and they remain applicable for more sparse and more intensive simulations.

### **Acknowledgments**

This work is supported by the Australian Research Council under grants DP120102294 and DP130100763.

## **6. APPENDIX: Original MMC**

The original MMC is a special case of generalised MMC, which is characterised by an important additional condition:  $n_c = n_r$ . This means that conditional variables coincide with the reference variables  $\boldsymbol{\eta} = \boldsymbol{\xi}$  since any selection of  $\boldsymbol{\eta} = \boldsymbol{\eta}(\boldsymbol{\xi}) \neq \boldsymbol{\xi}$  is equivalent to conditioning on  $\boldsymbol{\xi}$ ). While generalised MMC does not impose significant restrictions on the stochastic process emulating the conditioning variables (since any stochastic process can practically be approximated by Markov process of sufficiently large dimension), the Markov-family restrictions impose significant constraints on the reference variables in original MMC. Nevertheless, as a special case of generalised MMC, original MMC possesses all properties of generalised MMC and thus, is consistent with the pdf transport equation. In addition, the original MMC has some specific properties that are not applicable to generalised MMC. These properties are briefly discussed in this Appendix.

First, equation (21) takes the form

$$\frac{\partial Q_I P_\eta}{\partial t} + \nabla \cdot (\mathbf{U}_\eta Q_I P_\eta) + \frac{\partial A_i Q_I P_\eta}{\partial \eta_i} - \frac{\partial^2 B_{ij} Q_I P_\eta}{\partial \eta_i \partial \eta_j} - D \nabla^2 (Q_I P_\eta) = \langle W_I^* \rangle_\eta P_\eta \quad (24)$$

which is closed as long as we know how to evaluate the source term. The correlations of equation (21) are decoupled since all random variables  $\xi_i^*$  are present as conditions  $\xi_i^* = \eta_i$  in equation (24). Hence, the distinctive feature of original MMC is existence of a closed deterministic equation for  $Q$ , which is not the case for generalised MMC. The term  $D \nabla^2 (Q_I P_\eta)$  is small in high Reynolds flows and this term was neglected in original MMC [22]. The generalised MMC has only one formulation — stochastic with  $Y_I \cong Y_I^*$  (i.e. the reactive scalars  $Y_I$  are modelled by  $Y_I^*$ ); while the original MMC has two formulations: stochastic, where  $Y_I \cong Y_I^*$ , and deterministic, where  $Y_I \cong Q_I$ . This is related to another non-trivial point, which has been demonstrated for original MMC [22]: that modelling the reactive scalars by  $Q_I$  is also consistent with the pdf equation. If considered as a pdf model, the deterministic version of the original MMC represents a generalisation of the multidimensional Mapping Closure combined with CMC — this gave MMC its name of Multiple Mapping Conditioning.

## References

- [1] V. R. Kuznetsov, V. Sabel'nikov, Turbulence And Combustion, 1st Edition, Hemisphere Publishing Corporation, 1990.
- [2] P. Libby, F. Williams, Turbulent combustion: fundamental aspects and a review, Academic Press, London, 1994.
- [3] R. Bilger, Turbulent flows with nonpremixed reactants., in: P. Libby, F. Williams (Eds.), Turbulent Reacting Flows., Springer, 1980, Ch. 3, pp. 65–113.

- [4] A. Klimenko, R. Bilger, Conditional moment closure for turbulent combustion, *Progress in Energy and Combustion Science* 25 (1999) 595–687. doi:10.1016/S0360-1285(99)00006-4.
- [5] N. Peters, *Turbulent Combustion*, Cambridge University Press, 2000.
- [6] S. Pope, Pdf methods for turbulent reactive flows, *Progress in Energy and Combustion Science* 11 (1985) 119–192. doi:10.1016/0360-1285(85)90002-4.
- [7] D. Haworth, Progress in probability density function methods for turbulent reacting flows, *Progress in Energy and Combustion Science* 36. doi:10.1016/j.pecs.2009.09.003.
- [8] P. J. Colucci, F. A. Jaber, P. Givi, S. B. Pope, Filtered density function for large eddy simulation of turbulent reacting flows, *Physics of Fluids* 10 (1998) 499. doi:http://dx.doi.org/10.1063/1.869537.
- [9] R. Fox, *Computational Models for Turbulent Reacting Flows*, Cambridge University Press, United Kingdom, 2003.
- [10] S. Heinz, *Statistical Mechanics of Turbulent Flows*, Springer-Verlag, Berlin, 2003.
- [11] V. Raman, H. Pitsch, A consistent les/filtered-density function formulation for the simulation of turbulent flames with detailed chemistry, *Proceedings of the Combustion Institute* 31 (2007) 1711–1719. doi:doi:10.1016/j.proci.2006.07.152.
- [12] M. J. Cleary, A. Y. Klimenko, J. Janicka, M. Pfitzner, A sparse-lagrangian multiple mapping conditioning model for turbulent diffusion flames, in: *Proc. Combust. Inst.*, Vol. 32, 2009, p. 14991507.

- [13] S. Navarro-Martinez, A. Kronenburg, Les-cmc simulations of a lifted methane flame, *Proceedings of the Combustion Institute* 32 (2009) 1509–1516. doi:10.1016/j.proci.2008.06.178.  
URL <http://dx.doi.org/10.1016/j.proci.2008.06.178>
- [14] W. Jones, V. Prasad, Large eddy simulation of the sandia flame series (d - f) using the eulerian stochastic field method, *Combustion and Flame* 157 (2010) 1621–1636. doi:doi:10.1016/j.combustflame.2010.05.010.
- [15] T. Echekki, E. Mastorakos, *Turbulent Combustion Modelling. Advances, New Trends and Perspectives.*, Springer, 2011.
- [16] J. Villermaux, J. Devillon, Representation de la coalescence et de la re-dispersion des domaines de segregation dans un fluide par un modele d'interaction phenomenologique, *Proceedings of the second international symposium on chemical reaction engineering* (1972) 1–13.
- [17] C. Dopazo, E. O'Brien, An approach to the autoignition of a turbulent mixture, *Acta Astronautica* 1 (1974) 1239–1266.
- [18] R. Curl, Dispersed phase mixing: I. theory and effects in simple reactors, *AIChE Journal* 9 (1963) 175–181. doi:10.1002/aic.690090207.
- [19] J. Janicka, W. Kolbe, W. Kollmann, Closure of the transport equation for the probability density function of turbulent scalar fields., *Journal of Non-Equilibrium Thermodynamics* 4 (1977) 47–66.
- [20] R. Lindstedt, S. Louloudi, E. Vos, Joint scalar probability density function modeling of pollutant formation in piloted turbulent jet diffusion flames with comprehensive chemistry, *Proceedings of the Combustion Institute* 28 (2000) 149–156. doi:doi:10.1016/S0082-0784(00)80206-4.

- [21] S. Subramaniam, S. Pope, A mixing model for turbulent reactive flows based on euclidean minimum spanning trees, *Combustion and Flame* 115 (1998) 487–514. doi:10.1016/S0010-2180(98)00023-6.
- [22] A. Klimenko, S. Pope, The modeling of turbulent reactive flows based on multiple mapping conditioning, *Physics of Fluids* 15 (2003) 1907. doi:http://dx.doi.org/10.1063/1.1575754.
- [23] A. Klimenko, Matching conditional moments in pdf modelling of non-premixed combustion, *Combustion and Flame* 143 (2005) 369–385. doi:doi:10.1016/j.combustflame.2005.08.014.
- [24] M. Cleary, A. Klimenko, Multiple mapping conditioning: a new modelling framework for turbulent combustion., in: T. Echekki, E. Mastorakos (Eds.), *Turbulent Combustion Modelling. Advances, New Trends and Perspectives.*, Springer, 2011, Ch. 7, pp. 143–173.
- [25] A. P. Wandel, A. Y. Klimenko, Testing multiple mapping conditioning mixing for monte carlo probability density function simulations, *Physics of Fluids* 17 (2005) 128105. doi:http://dx.doi.org/10.1063/1.2147609.
- [26] M. Cleary, A. Kronenburg, Multiple mapping conditioning for extinction and reignition in turbulent diffusion flames, *Proceedings of the Combustion Institute* 31 (2007) 1497–1505. doi:doi:10.1016/j.proci.2006.07.215.
- [27] K. Vogiatzaki, M. Cleary, A. Kronenburg, J. Kent, Modeling of scalar mixing in turbulent jet flames by multiple mapping conditioning, *Physics of Fluids* 21. doi:10.1063/1.3081553.  
URL <http://dx.doi.org/10.1063/1.3081553>
- [28] K. Vogiatzaki, A. Kronenburg, S. Navarro-Martinez, W. Jones, Stochastic multiple mapping conditioning for a piloted, turbulent jet diffusion

- flame, *Proceedings of the Combustion Institute* 33 (2011) 1523–1531.  
doi:10.1016/j.proci.2010.06.126.  
URL <http://dx.doi.org/10.1016/j.proci.2010.06.126>
- [29] P. Vaishnavi, A. Kronenburg, Multiple mapping conditioning of velocity in turbulent jet flames, *Combustion and Flame* 157 (2010) 1863–1865.  
doi:10.1016/j.combustflame.2010.06.007.
- [30] C. B. Devaud, I. Stankovic, B. Merci, Deterministic multiple mapping conditioning (MMC) applied to a turbulent flame in Large Eddy Simulation (LES), *Proceedings of the Combustion Institute* 34 (1) (2013) 1213–1221.
- [31] S. Pope, A model for turbulent mixing based on shadow-position conditioning, *Physics of Fluids* 25. doi:<http://dx.doi.org/10.1063/1.4818981>.
- [32] A. P. Wandel, R. P. Lindstedt, Hybrid multiple mapping conditioning modeling of local extinction, *Proceedings of the Combustion Institute* 34 (1) (2013) 1365–1372.
- [33] B. Sundaram, A. Y. Klimenko, M. J. Cleary, U. Maas, Prediction of NO<sub>x</sub> in premixed high-pressure lean methane flames with a MMC-partially stirred reactor, *Proceedings of the Combustion Institute* 35 (2) (2015) 1517–1525.
- [34] M. J. Cleary, A. Y. Klimenko, A generalised multiple mapping conditioning approach for turbulent combustion, *Flow, Turbulence and Combustion* 82 (2009) 477–491.
- [35] A. Y. Klimenko, Lagrangian particles with mixing. II. sparse-lagrangian methods in application for turbulent reacting flows, *Phys. Fluids* 21 (2009) 065102.
- [36] Y. Ge, M. Cleary, A. Klimenko, A comparative study of Sandia flame series

- (df) using sparse-lagrangian MMC modelling, *Proceedings of the Combustion Institute* 34 (2013) 1325–1332. doi:doi:10.1016/j.proci.2012.06.059.
- [37] A. Norris, S. Pope, Turbulent mixing model based on ordered pairing, *Combustion and Flame* 83 (1991) 27–42. doi:doi:10.1016/0010-2180(91)90201-L.
- [38] R. Barlow, J. Frank, Effects of turbulence on species mass fractions in methane/air jet flames, *Symposium (International) on Combustion* 27 (1998) 1087–1095. doi:doi:10.1016/S0082-0784(98)80510-9.
- [39] R. Cabra, T. Myhrvold, J. Chen, R. Dibble, A. Karpetis, R. Barlow, Simultaneous laser raman-rayleigh-lif measurements and numerical modeling results of a lifted turbulent  $\text{H}_2/\text{N}_2$  jet flame in a vitiated coflow, *Proceedings of the Combustion Institute* 29 (2002) 1881–1888. doi:doi:10.1016/S1540-7489(02)80228-0.
- [40] L. Dialameh, M. Cleary, A. Klimenko, A multiple mapping conditioning model for differential diffusion, *Physics of Fluids* 26. doi:http://dx.doi.org/10.1063/1.4864101.
- [41] A. Y. Klimenko, Mmc modelling and fluctuations of the scalar dissipation, in: *2003 Australian Symposium on Combustion & The 8th Australian Flame Days, 2003*.
- [42] A. Klimenko, Matching the conditional variance as a criterion for selecting parameters in the simplest multiple mapping conditioning models, *Combustion and Flame* 16 (2004) 4754–4757. doi:doi:10.1016/j.combustflame.2005.08.014.
- [43] R. O. Fox, On velocityconditioned scalar mixing in homogeneous turbulence, *Physics of Fluids* 8 (1996) 2678–2691. doi:http://dx.doi.org/10.1063/1.869054.

- [44] Y. Ge, M. Cleary, A. Klimenko, Sparse-lagrangian fdf simulations of Sandia flame E with density coupling, *Proceedings of the Combustion Institute* 33. doi:doi:10.1016/j.proci.2010.06.035.
- [45] A. Y. Klimenko, On simulating scalar transport by mixing between Lagrangian particles, *Phys. Fluids* 19 (2007) 031702.
- [46] A. Y. Klimenko, M. J. Cleary, Convergence to a model in sparse-lagrangian fdf simulations, *Flow, Turbulence and Combustion* 85 (2010) 567591.
- [47] A. Y. Klimenko, Lagrangian particles with mixing. I. simulating scalar transport, *Phys. Fluids* 21 (2009) 065101.
- [48] K. Vogiatzaki, S. Navarro-Martinez, S. De, A. Kronenburg, Mixing modelling framework based on multiple mapping conditioning for the prediction of turbulent flame extinction, *Flow Turbulence Combust* (2015) to appear.
- [49] M. Cleary, A. Klimenko, A detailed quantitative analysis of sparse-lagrangian filtered density function simulations in constant and variable density reacting jet flows, *Physics of Fluids* 23. doi:http://dx.doi.org/10.1063/1.3657085.
- [50] A. Y. Klimenko, On the relation between the conditional moment closure and unsteady flamelets, *Combustion Theory and Modelling* 5 (2001) 275–294. doi:10.1088/1364-7830/5/3/302.
- [51] A. Kempf, F. Flemming, J. Janicka, Investigation of lengthscales, scalar dissipation, and flame orientation in a piloted diffusion flame by les, *Proceedings of the Combustion Institute* 30 (1) (2005) 557–565.
- [52] Y. Ge, Generalised multiple mapping conditioning for turbulent combustion simulation, Ph.D. thesis, University of Queensland (2012).

- [53] G. Smith, D. Golden, M. Frenklach, N. Moriarty, B. Eiteneer, M. Goldenberg, C. Bowman, R. Hanson, S. Song, W. G. Jr., V. Lissianski, Z. Qin, Gri-mech 3.0.  
URL [http://www.me.berkeley.edu/gri\\_mech/](http://www.me.berkeley.edu/gri_mech/)
- [54] R. Gordon, S. Starner, A. Masri, R. Bilger, Further characterisation of lifted hydrogen and methane flames issuing into a vitiated coflow, 5th Asia-Pacific Conference on Combustion ASPACC 2005.
- [55] Z. Wu, S. Starner, R. Bilger, Lift-off heights of turbulent  $\text{H}_2/\text{N}_2$  jet flames in a vitiated co-flow, Proceedings of the 2003 Australian Symposium on Combustion and the Eighth Australian Flame Days.
- [56] R. R. Cao, S. B. Pope, A. R. Masri, Turbulent lifted flames in a vitiated coflow investigated using joint pdf calculations, *Combustion and Flame* 142 (2005) 438–453. doi:doi:10.1016/j.combustflame.2005.04.005.
- [57] M. A. Mueller, T. J. Kim, R. A. Yetter, F. L. Dryer, Flow reactor studies and kinetic modeling of the  $\text{H}_2/\text{O}_2$  reaction, *International Journal of Chemical Kinetics* 31 (1999) 113–125. doi:DOI: 10.1002/(SICI)1097-4601.
- [58] S. Navarro-Martinez, A. Kronenburg, Flame stabilization mechanisms in lifted flames, *Flow, Turbulence and Combustion* 87 (2011) 377–406. doi:10.1007/s10494-010-9320-1.
- [59] R. A. Yetter, F. L. Dryer, H. Rabitz, A comprehensive reaction mechanism for carbon monoxide/hydrogen/oxygen kinetics, *Combustion Science and Technology* 79 (1991) 97–128. doi:10.1080/00102209108951759.
- [60] J. Li, Z. Zhao, A. Kazakov, F. L. Dryer, An updated comprehensive kinetic model of hydrogen combustion, *International Journal of Chemical Kinetics* 36 (2004) 566–575. doi:DOI: 10.1002/kin.20026.

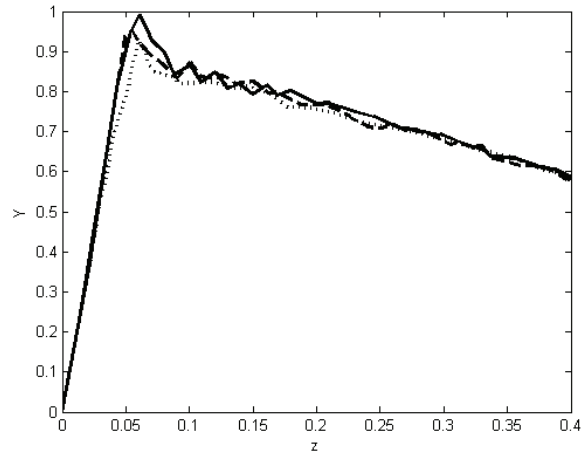


Figure 1: Convergence test for the one step flamesheet case, with 1L/32E (dotted line), double (dashed line) and quadruple (solid line) the number of particles with the same mixing distances between particles for each simulation. Conditional mean of the burning index ( $Y$ ) versus Lagrangian mixture fraction ( $z$ ) are shown for the three simulations at  $x/d = 13$ .

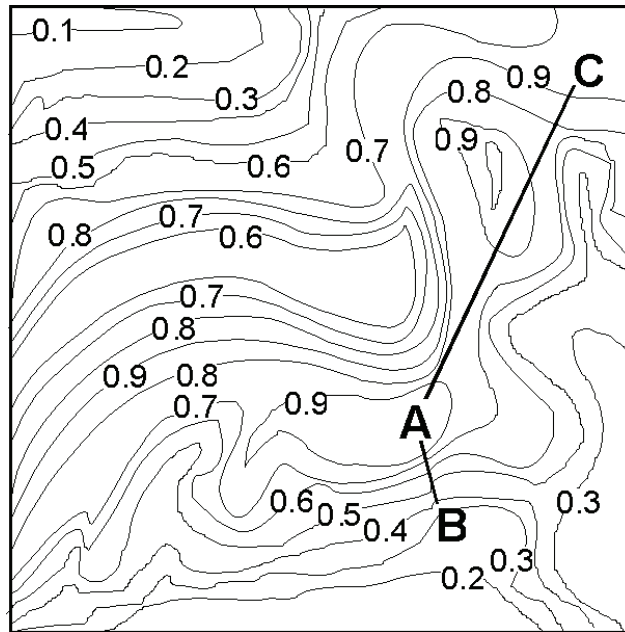


Figure 2: Schematic of generalised MMC localisation with a contour plot of the Eulerian filtered mixture fraction field with Lagrangian particles A, B and C.

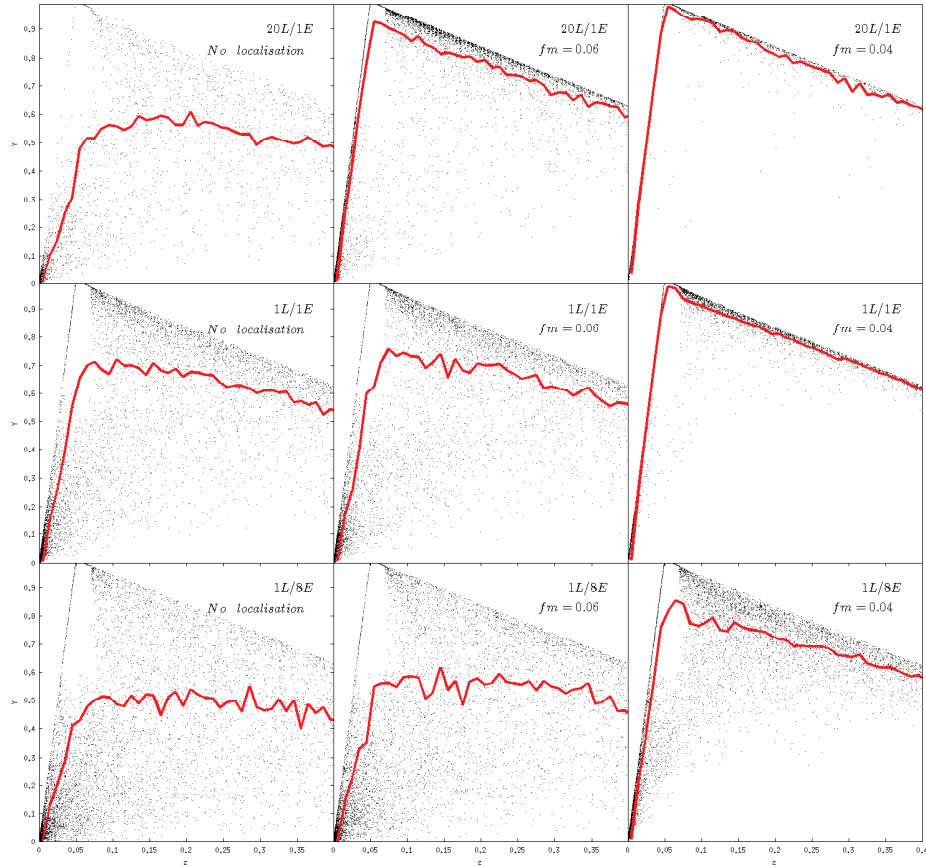


Figure 3: Scatter plots (black dots) and conditional means (red line) of the burning index ( $Y$ ) versus Lagrangian mixture fraction ( $z$ ) at  $x/d = 9$  for the one-step flamesheet case. Top row: 20 Lagrangian particles per LES cell (20L/1E), middle row: 1L/1E and bottom row: 1L/8E. Left column: No localisation, middle column:  $f_m = 0.06$  and right column:  $f_m = 0.04$  [49].

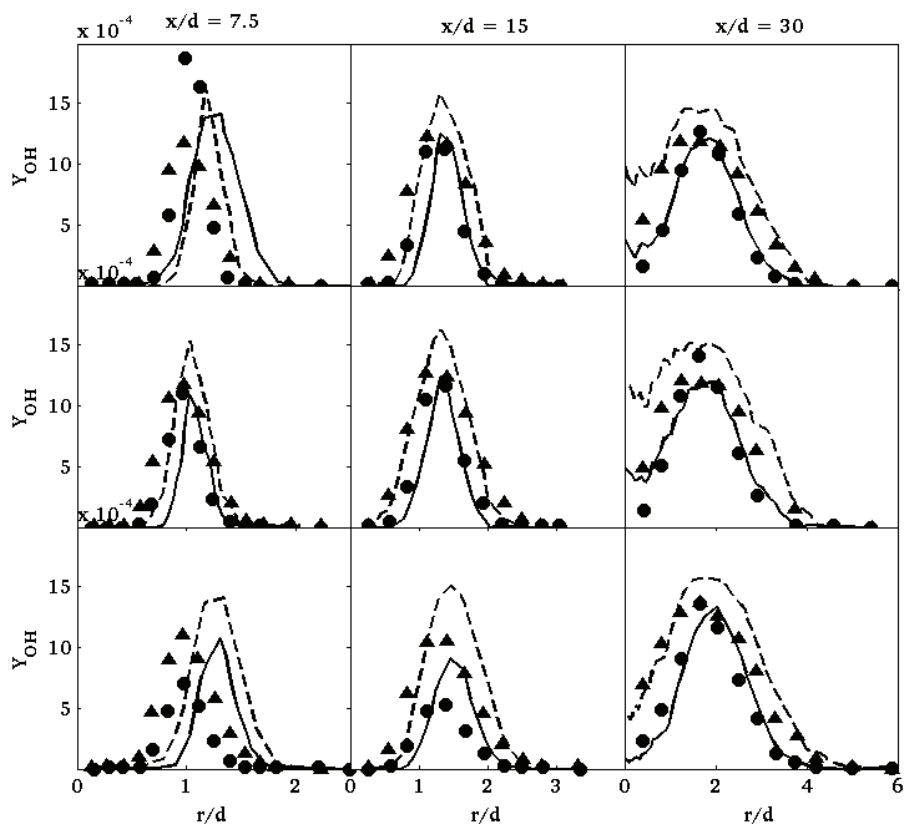


Figure 4: Radial profiles of steady-state unconditional mean OH for the Sandia flame series [38]. Top row: Flame D, middle row: flame E, bottom row: flame F. Circles: experimental mean, triangles: experimental rms. Solid line: simulated mean, dashed line: simulated rms.

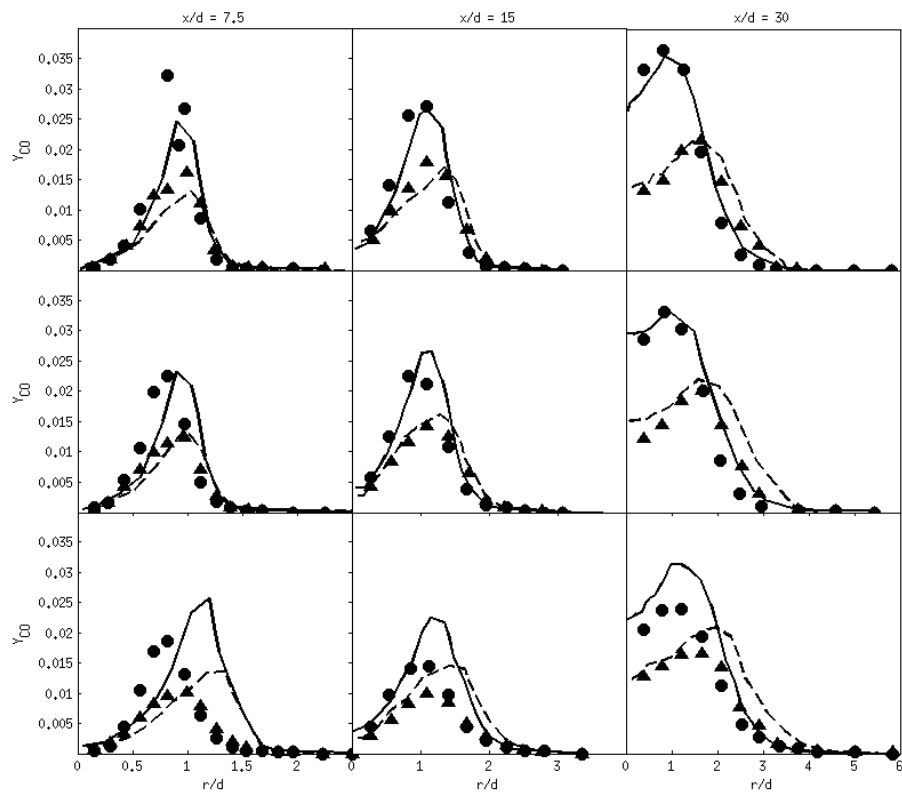


Figure 5: Radial profiles of steady-state unconditional mean CO for the Sandia flame series [38]. Top row: Flame D, middle row: flame E, bottom row: flame F. Circles: experimental mean, triangles: experimental rms. Solid line: simulated mean, dashed line: simulated rms.

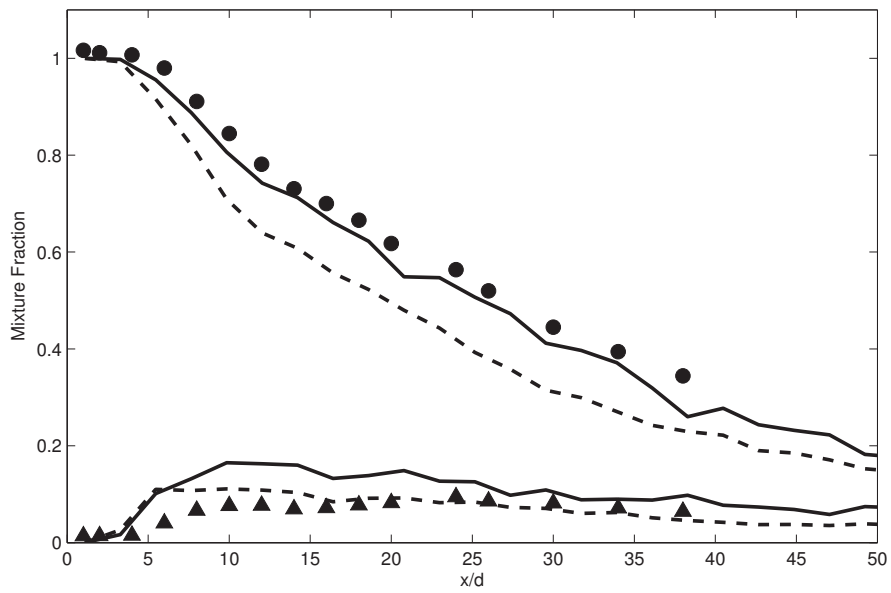


Figure 6: Steady-state axial mean and rms mixture fraction profile for the Cabra lifted hydrogen flame [39]. Circles: experimental mean, triangles: experimental rms. Solid line: Lagrangian mixture fraction, dashed line: Eulerian mixture fraction.

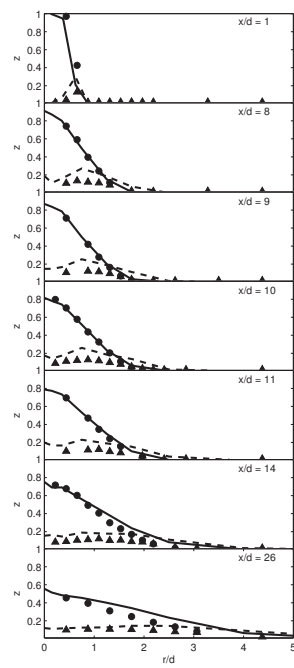


Figure 7: Radial mixture fraction profiles at various axial locations for the Cabra lifted hydrogen flame [39]. Symbols: experimental data; solid line: Lagrangian mean mixture fraction, dashed line: Lagrangian RMS mixture fraction.

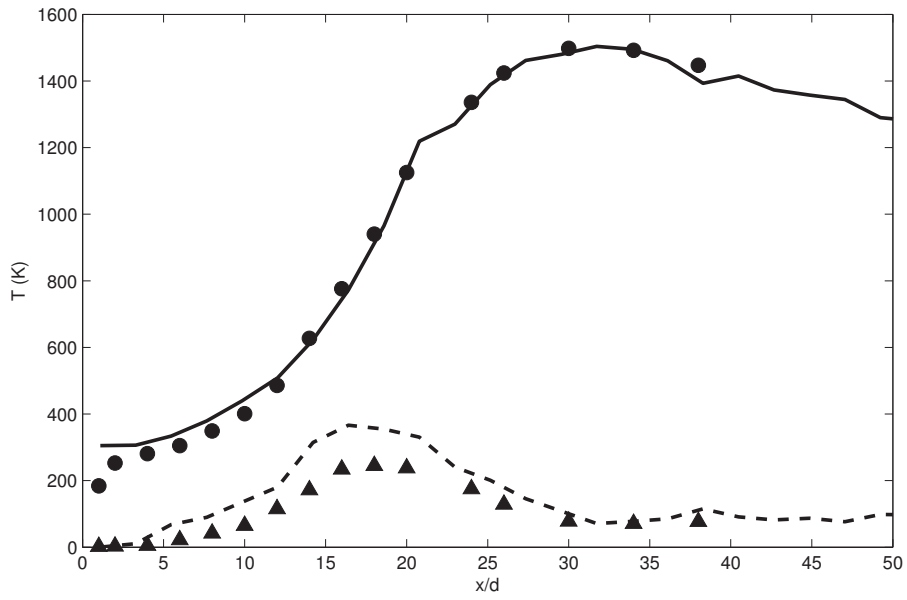


Figure 8: Steady-state axial temperature profile for the Cabra lifted hydrogen flame [39]. Circles: experimental mean, triangles: experimental rms. Solid line: Simulated mean temperature, dashed line: simulated RMS temperature.

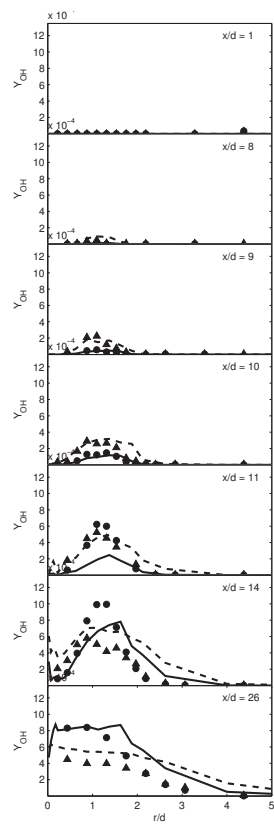


Figure 9: Radial mean OH profiles at various axial locations for the Cabra lifted hydrogen flame [39]. Circles: experimental data; solid line: Simulation results.

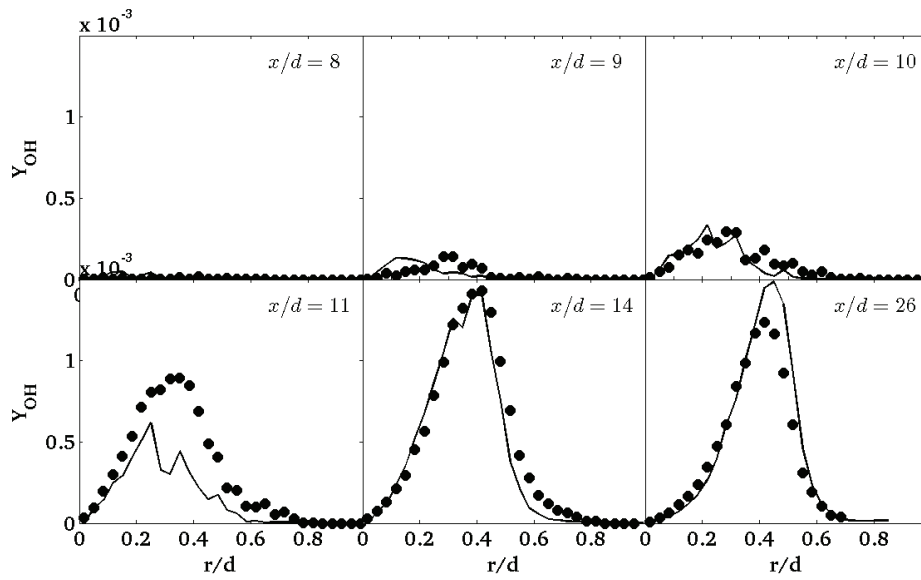


Figure 10: Conditional mean OH profiles at various axial locations for the Cabra lifted hydrogen flame [39]. Circles: experimental data; solid line: Simulation results.

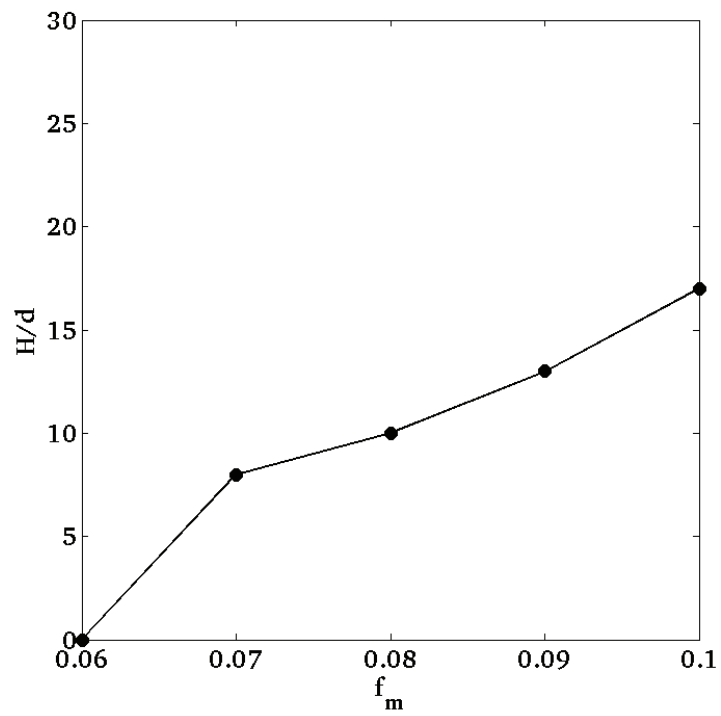


Figure 11: Lift-off height versus localisation parameter for the Cabra lifted hydrogen flame.

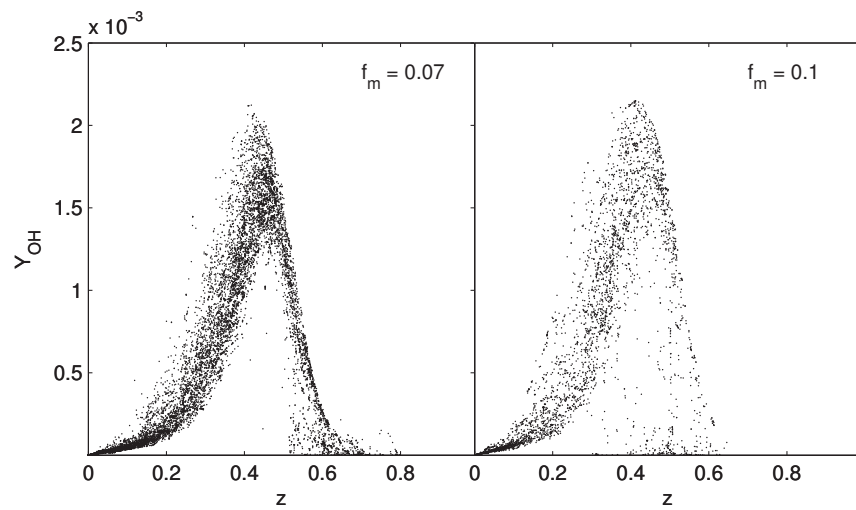


Figure 12: Scatterplots of OH at  $x/d = 26$  for two values of  $f_m$  for the Cabra lifted hydrogen flame.